

Constraints on axion and corrections to Newtonian gravity from the Casimir effect*

G. L. Klimchitskaya^{†1,2} and V. M. Mostepanenko^{‡1,2}

¹*Central Astronomical Observatory at Pulkovo of the Russian Academy of Sciences, St.Petersburg, 196140, Russia*

²*Institute of Physics, Nanotechnology and Telecommunications, St.Petersburg State Polytechnical University, St.Petersburg, 195251, Russia*

Abstract

Axion is a light pseudoscalar particle of much interest for physics of elementary particles and for astrophysics. We review the recently obtained constraints on axion to nucleon coupling constants following from different experiments on measuring the Casimir interaction. These constraints are compared with those following from other laboratory experiments within the wide range of masses of axion-like particles from 10^{-10} to 20 eV. We also collect the most strong constraints on the Yukawa-type and power-type corrections to the Newton law of gravitation which follow from measurements of the Casimir interaction, Eötvos- and Cavendish-type experiments. The possibility to obtain stronger constraints on an axion from the Casimir effect is proposed.

PACS numbers: 14.80.Va, 12.20.Fv, 14.80.-j

* Based on two talks presented by V. M. Mostepanenko and G. L. Klimchitskaya at the 15th Russian Gravitational Conference — International Conference on Gravitation, Cosmology and Astrophysics (RUSGRAV-15). June 30–July 5, 2014. Kazan, Russia.

† E-mail: g.klimchitskaya@gmail.com

‡ E-mail: vmostepa@gmail.com

I. INTRODUCTION

The light pseudoscalar particle named *axion* is an important element of the Standard Model and its generalizations. Axion arises [1, 2] due to breaking of the Peccei-Quinn symmetry which was introduced [3] in quantum chromodynamics (QCD) in order to avoid strong *CP* violation and large electric dipole moment of a neutron (numerous experiments exclude both these effects to a high level of precision). What is more, axions provide an elegant solution for the problem of dark matter in astrophysics and cosmology [4, 5]. This is the reason why a lot of experiments for searching axions has been performed in different countries [6]. Specifically, strong constraints on the coupling constants of an axion and other axion-like particles with photons, electrons and nucleons were obtained from astrophysical observations. Up to the present, however, there is the so-called *window* in the values of an axion mass, where these constraints are either missing or not sufficiently strong.

There are also massless and light scalar particles predicted in many extensions of the Standard Model [7]. Exchange of such particles between atoms of two macrobodies leads to corrections to the Newton law of gravitation at separations below a micrometer. By coincidence, at so small separations Newton's gravitational law is not verified experimentally with sufficient precision. Within a submicrometer interaction range experiment does not exclude corrections which exceed the Newton gravitational force by many orders of magnitude [8]. Similar corrections are predicted in extra-dimensional models with a low-energy compactification scale [9, 10]. Many experiments of Eötvos- and Cavendish-type have been performed during the last few years searching for possible corrections to the Newton law of gravitation [11].

Recently it was found [12–15] that strong model-independent constraints on the coupling constants of axions with nucleons follow from measurements of the Casimir-Polder and Casimir force. Some of these constraints overlap with an axion window and, thus, are complementary to astrophysical limits. As to corrections to Newton's law of gravitation, measurements of the van der Waals and Casimir forces have long been used to constrain their parameters [16, 17]. New, more precise measurements of the Casimir force allowed significant strengthening of previously obtained constraints on non-Newtonian gravity over the region of separations below $1\ \mu\text{m}$ [18–22].

In this paper, we review constraints on the coupling constants of an axion to a proton

and a neutron, and corrections to Newton's law of gravitation which follow from the most precise measurements of the Casimir interaction [23, 24]. We compare the obtained constraints on an axion with the alternative constraints following from some other laboratory experiments. The constraints on the coupling constants of an axion and on non-Newtonian gravity, following from measurements of the Casimir interaction, are mutually compared and some conclusions inherent to both of them are obtained.

The paper is organized as follows. In Section 2 we consider the types of effective potentials which arise due to one- and two-axion exchange. These are compared with the effective potentials originating from the exchange of massless and massive scalar particles. Section 3 is devoted to the constraints on axion-nucleon coupling constants which follow from measurements of the Casimir-Polder force acting between the condensate of ^{87}Rb atoms and a glass silica plate. In Section 4 the constraints on axion to nucleon coupling constants are presented obtained from measurements of the gradient of the Casimir force between a microsphere and a plate coated with a nonmagnetic metal Au or a magnetic metal Ni. These experiments were performed by means of a dynamic atomic force microscope (AFM). Section 5 contains similar constraints obtained from measurements of the gradient of the Casimir force between Au-coated surfaces of a sphere and a plate using a micromachined oscillator. In Section 6 the constraints on the coupling constants of an axion are provided which follow from measurements of the Casimir force between corrugated surfaces. In Section 7 we compare the constraints on an axion found from measurements of the Casimir interaction with those obtained from some other laboratory experiments. Section 8 is devoted to the constraints on non-Newtonian gravity derived from the Casimir effect. In Section 9 the reader will find our conclusions and discussion.

Throughout the paper we use units in which $\hbar = c = 1$.

II. TYPES OF EFFECTIVE POTENTIALS

Below we consider effective potentials arising from the interaction of nucleons (protons and neutrons) with an axion and other axion-like particles predicted in different variants of the Grand Unification Theories. Axions also interact with electrons and photons. These interactions are, however, much weaker than axion-nucleon interaction [25] and for our purposes can be neglected. In any case, their account would lead to only a minor strengthening

of the constraints on axion-nucleon coupling constants obtained from the force measurements between macroscopic bodies.

We assume that the interaction of axion-like particles a with nucleons ψ is described by the Lagrangian [4]

$$\mathcal{L} = -ig_{ak}\bar{\psi}\gamma_5\psi a, \quad (1)$$

where g_{ak} is the coupling constant of an axion to a proton ($k = p$) or to a neutron ($k = n$). In doing so the pseudoscalar coupling of axions and other axion-like particles to nucleons is assumed (note that the pseudovector coupling introduced for the original QCD axions results in the nonrenormalizable theory [15]). The exchange of one axion between two nucleons of spins $\boldsymbol{\sigma}_{1,2}/2$ situated at the points $\mathbf{r}_1 \neq \mathbf{r}_2$ with coupling (1) results in the following effective potential [25, 26]

$$\begin{aligned} V(\mathbf{r}_1 - \mathbf{r}_2; \boldsymbol{\sigma}_1, \boldsymbol{\sigma}_2) &= \frac{g_{ak}g_{al}}{16\pi m_k m_l} \left[(\boldsymbol{\sigma}_1 \cdot \mathbf{n})(\boldsymbol{\sigma}_2 \cdot \mathbf{n}) \right. \\ &\quad \times \left(\frac{m_a^2}{|\mathbf{r}_1 - \mathbf{r}_2|} + \frac{3m_a}{|\mathbf{r}_1 - \mathbf{r}_2|^2} + \frac{3}{|\mathbf{r}_1 - \mathbf{r}_2|^3} \right) \\ &\quad \left. - (\boldsymbol{\sigma}_1 \cdot \boldsymbol{\sigma}_2) \left(\frac{m_a}{|\mathbf{r}_1 - \mathbf{r}_2|^2} + \frac{1}{|\mathbf{r}_1 - \mathbf{r}_2|^3} \right) \right] e^{-m_a|\mathbf{r}_1 - \mathbf{r}_2|}. \end{aligned} \quad (2)$$

Here, g_{ak} and g_{al} are the axion-proton ($k, l = p$) or axion-neutron ($k, l = n$) interaction constants, m_k, m_l are the nucleon masses, m_a is the axion mass, and the unit vector $\mathbf{n} = (\mathbf{r}_1 - \mathbf{r}_2)/|\mathbf{r}_1 - \mathbf{r}_2|$.

As is seen in (2), the effective potential depends on the nucleon spins. Because of this, the resulting interaction between two unpolarized test bodies averages to zero. Taking into account that already performed experiments on measuring the Casimir interaction [23, 24] deal with unpolarized test bodies, it seems impossible to use them for constraining the axion to nucleon coupling constants basing on the simplest process of one-axion exchange.

The situation changes when we consider the process of two-axion exchange between the two nucleons. In this case the Lagrangian (1) leads to the following effective potential [25, 27, 28]

$$V_{kl}(|\mathbf{r}_1 - \mathbf{r}_2|) = -\frac{g_{ak}^2 g_{al}^2}{32\pi^3 m_k m_l} \frac{m_a}{(|\mathbf{r}_1 - \mathbf{r}_2|)^2} K_1(2m_a|\mathbf{r}_1 - \mathbf{r}_2|), \quad (3)$$

where $K_1(z)$ is the modified Bessel function of the second kind. Note that (3) is derived under the condition $|\mathbf{r}_1 - \mathbf{r}_2| \gg 1/m_{k,l}$ which is satisfied with a large safety margin in all the experiments considered below. Equation (3) does not depend on the nucleon spins. Thus,

after the integration over the volumes of test bodies, it leads to some additional force of the axionic origin which can be constrained from the measurement results.

Now we address to exchange of massless and light scalar particles between the atoms of two macroscopic bodies. The exchange of one light scalar particle of mass M between two pointlike particles with masses m_1 and m_2 spaced at the points \mathbf{r}_1 and \mathbf{r}_2 results in the spin-independent Yukawa-type effective potential [8]. It is convenient to parametrize this potential as a correction to Newton's law of gravitation:

$$V(|\mathbf{r}_1 - \mathbf{r}_2|) = -\frac{Gm_1m_2}{|\mathbf{r}_1 - \mathbf{r}_2|} (1 + \alpha e^{-|\mathbf{r}_1 - \mathbf{r}_2|/\lambda}). \quad (4)$$

Here, α is a dimensionless constant characterizing the strength of Yukawa interaction, $\lambda = 1/M$ is the Compton wavelength of light scalar particle characterizing the interaction range, and G is the Newtonian gravitational constant. As was noted in Section 1, the effective potential (4) arises also in extradimensional models with a low-energy compactification scale [9, 10]. In this case the quantity λ has the meaning of the characteristic size of a multidimensional compact manifold.

The exchange of one massless scalar particle leads to an effective potential which is inversely proportional to the separation distance. The exchange of an even number of massless pseudoscalar particles (for instance, by the arions) results in the effective potentials inversely proportional to higher powers of the separation. Similar potentials arise also due to the exchange of two neutrinos, two goldstinos, or other massless fermions [29, 30]. The power-type effective potentials are also usually parametrized as corrections to Newton's law of gravitation

$$V_n(|\mathbf{r}_1 - \mathbf{r}_2|) = -\frac{Gm_1m_2}{|\mathbf{r}_1 - \mathbf{r}_2|} \left[1 + \Lambda_n \left(\frac{r_0}{|\mathbf{r}_1 - \mathbf{r}_2|} \right)^{n-1} \right]. \quad (5)$$

Here, Λ_n is a dimensionless constant, n is a positive integer, and $r_0 = 10^{-15}$ m is chosen to preserve the correct dimension of energy at different n . Note that the exchange by two axion-like particles in the limiting case $m_a \rightarrow 0$ in accordance to (3) results in the potential [31]

$$V_{kl}(|\mathbf{r}_1 - \mathbf{r}_2|) = -\frac{g_{ak}^2 g_{al}^2}{64\pi^3 m_k m_l} \frac{1}{|\mathbf{r}_1 - \mathbf{r}_2|^3}. \quad (6)$$

This can be represented as a correction to Newton's law of gravitation in (5) with $n = 3$ (the same power-type interaction is obtained from the exchange of two arions). The effective potential (5) with $n = 3$ is also obtained from extra-dimensional models with noncompact (but warped) extra dimensions [32, 33].

III. CONSTRAINTS ON AN AXION FROM MEASUREMENTS OF THE CASIMIR-POLDER FORCE

The Casimir-Polder force acting between ^{87}Rb atoms belonging to a Bose-Einstein condensate cloud and a SiO_2 plate was measured by means of the following dynamic experiment [34]. The condensate cloud was placed in a magnetic trap with frequencies $\omega_{0z} = 1438.85 \text{ rad/s}$ in the perpendicular direction to the plate and $\omega_{0t} = 40.21 \text{ rad/s}$ in the lateral direction. The Thomas-Fermi radii of the condensate cloud of ^{87}Rb atoms in the perpendicular and lateral directions were $R_z = 2.69 \mu\text{m}$ and $R_l = 97.1 \mu\text{m}$, respectively. The dipole oscillations of the condensate in the z direction with a constant amplitude $A_z = 2.5 \mu\text{m}$ were excited. The separation distance a between the center of mass of a condensate and a plate was varied from 6.88 to 11 μm , i.e., in the region where the thermal effects in the Casimir-Polder force contribute essentially. The temperature of the plate was equal to either $T = 310 \text{ K}$ (as in an environment) or $T = 479 \text{ K}$ and $T = 605 \text{ K}$ (which corresponds to out of equilibrium situations). However, for constraining the parameters of an axion, the strongest result follows from the measurements in thermal equilibrium.

Under the influence of the Casimir-Polder force between ^{87}Rb atoms and a plate, the oscillation frequency ω_{0z} slightly shifts to some other value ω_z . The relative frequency shift is given by

$$\gamma_z = \frac{|\omega_{0z} - \omega_z|}{\omega_{0z}} \approx \frac{|\omega_{0z}^2 - \omega_z^2|}{2\omega_{0z}^2}. \quad (7)$$

This frequency shift was measured [34] as a function of a with some measurement errors determined at a 67% confidence level. For example, at the shortest separation $a_1 = 6.88 \mu\text{m}$ this absolute error was $\Delta_1 \gamma_z = 3.06 \times 10^{-5}$. The quantity γ_z was also calculated using the Lifshitz theory of atom-wall interaction and subsequent averaging over the condensate cloud. Under the assumption that SiO_2 is an ideal insulator, i.e., by disregarding the influence of its dc conductivity, it was found [34] that the measurement results are in agreement with theory in the limits of the experimental error $\Delta \gamma_z$ (the importance of this assumption was demonstrated later [23, 24, 35]).

Due to the interaction potential (3), there may be also some additional force between a condensate cloud and a plate caused by the two-axion exchange between protons and neutrons belonging to them. The respective additional frequency shift can be calculated by the additive summation of (3) over all nucleons of a ^{87}Rb atom and a plate with subsequent

averaging over the condensate cloud (see [12] for details). Under an assumption that the plate has an infinitely large area (it was shown [12] that relative corrections to the result due to a finite plate area are of order 10^{-6}) the additional frequency shift due to two-axion exchange is given by [12]

$$\gamma_z^{\text{add}}(a) = \frac{15A(g_{ap}, g_{an})}{2\pi A_z m_{\text{Rb}} \omega_{0z}^2} \Phi(a, m_a), \quad (8)$$

where m_{Rb} is the mass of ^{87}Rb atom and the function $\Phi(a, m_a)$ is defined as

$$\begin{aligned} \Phi(a, m_a) &= \int_1^\infty du \frac{\sqrt{u^2 - 1}}{u} e^{-2m_a a u} \\ &\times (1 - e^{-2m_a D u}) I_1(2m_a A_z u) \Theta(2m_a R_z u). \end{aligned} \quad (9)$$

Here, $D = 7$ mm is the thickness of SiO_2 plate and

$$\Theta(t) \equiv \frac{1}{t^3} (t^2 \sinh t - 3t \cosh t + 3 \sinh t). \quad (10)$$

The constant $A(g_{ap}, g_{an})$ in (8) depends on the material properties as follows [12]

$$\begin{aligned} A(g_{ap}, g_{an}) &= \frac{\rho_{\text{SiO}_2} m_a}{16\pi^2 m^2 m_{\text{H}}} (37g_{ap}^2 + 50g_{an}^2) \\ &\times \left(\frac{Z_{\text{SiO}_2}}{\mu_{\text{SiO}_2}} g_{ap}^2 + \frac{N_{\text{SiO}_2}}{\mu_{\text{SiO}_2}} g_{an}^2 \right), \end{aligned} \quad (11)$$

where ρ_{SiO_2} is the plate density, $m = (m_p + m_n)/2$ is the mean nucleon mass, Z_{SiO_2} and N_{SiO_2} are the number of protons and the mean number of neutrons in a SiO_2 molecule, respectively. The quantity $\mu_{\text{SiO}_2} = m_{\text{SiO}_2}/m_{\text{H}}$, where m_{SiO_2} is the mean mass of a SiO_2 molecule and m_{H} is the mass of atomic hydrogen.

Taking into account that the observed frequency shift was in agreement with that originating from the Casimir-Polder force, the additional frequency shift (8) due to two-axion exchange should be constrained by the magnitude of the experimental error

$$\gamma_z^{\text{add}}(a_1) \leq \Delta_1 \gamma_z. \quad (12)$$

From the numerical analysis of this equation, the constraints on axion-nucleon coupling constants were obtained [12] under different assumptions about a relationship between g_{an} and g_{ap} . For example, under a natural assumption that $g_{an} = g_{ap}$ [25], the resulting constraints are shown in Fig. 1, where the region of the plane above the line is excluded and the region below the line is allowed. These constraints cover the wide region of axion masses from $m_a = 10^{-4}$ to 0.3 eV. As is seen in Fig. 1, the strength of constraints decreases with increasing axion mass. In Section 7 we compare the constraints of Fig. 1 with those obtained from other measurements of the Casimir force and different laboratory experiments.

IV. CONSTRAINTS ON AN AXION FROM MEASUREMENTS OF THE GRADIENT OF THE CASIMIR FORCE BY MEANS OF AFM

In the sequence of three experiments, the gradient of the Casimir force was measured between the surfaces of a hollow sphere and a plate both coated with Au films [36, 37], with Au and Ni films, respectively [38], and with Ni films [39, 40]. For technological purposes, there were also various material layers below Au and Ni coatings on both a hollow sphere made of fused silica (SiO_2) and a sapphire (Al_2O_3) plate. The radii of spheres were of about $50\ \mu\text{m}$ and the plates (disks) were of approximately 5 mm radius, i.e., by a factor of 100 larger than the spheres. Measurements of the gradient of the Casimir force, $\partial F_C(a)/\partial a$, as a function of separation a between the plate and the sphere, were performed by means of dynamic AFM (see [36, 37] for details). In all three experiments the measurement results were found in agreement with theoretical predictions of the Lifshitz theory in the limits of the experimental errors $\Delta F'_C(a)$. Calculations of the theoretical force gradients were performed with omitted relaxation properties of conduction electrons in metals (an account of the relaxation properties of conduction electrons in computations using the Lifshitz theory leads to disagreement with the measurement data of many experiments [22–24, 36, 37, 39, 40]).

The two-axion exchange between nucleons belonging to a sphere and a plate leads to some attraction in addition to the Casimir force. The gradient of this additional force acting between a spherical envelope (layer) of thickness Δ_s and external radius R , and a plate of thickness D can be calculated by the additive summation of the interaction potentials (3) [13]

$$\begin{aligned} \frac{\partial F_{\text{add}}(a)}{\partial a} &= \frac{\pi}{m^2 m_H^2} C_p C_s \int_1^\infty du \frac{\sqrt{u^2 - 1}}{u^2} (1 - e^{-2m_a u D}) \\ &\times e^{-2m_a a u} [\Phi(R, m_a u) - e^{-2m_a u \Delta_s} \Phi(R - \Delta_s, m_a u)], \end{aligned} \quad (13)$$

where the function $\Phi(r, z)$ is defined as

$$\Phi(r, z) = r - \frac{1}{2z} + e^{-2rz} \left(r + \frac{1}{2z} \right), \quad (14)$$

the coefficients $C_{p(s)}$ for a plate (spherical layer) materials are given by

$$C_{p(s)} = \rho_{p(s)} \left(\frac{g_{ap}^2}{4\pi} \frac{Z_{p(s)}}{\mu_{p(s)}} + \frac{g_{an}^2}{4\pi} \frac{N_{p(s)}}{\mu_{p(s)}} \right), \quad (15)$$

$\rho_{p(s)}$ are the plate (spherical layer) densities, and the quantities $Z_{p(s)}$, $N_{p(s)}$ and $\mu_{p(s)}$ have the same meaning, as explained below (11), but in application to the molecules (atoms) of a plate and a spherical layer, respectively.

Now we concentrate our attention on the experiment using Au-coated surfaces of a spherical envelope of thickness $\Delta_s^g = 5 \mu\text{m}$, of radius $R = 41.3 \mu\text{m}$ and a plate [36, 37]. The thicknesses of the Au coating on the sphere and the plate were $\Delta_s^{\text{Au}} = \Delta_p^{\text{Au}} = 280 \text{ nm}$. This allows to calculate the Casimir force (but not the additive force due to two-axion exchange) as between entirely Au bodies. In calculation of the additional force it should be taken into account that in the experiment [36, 37] the Au layers on both the spherical envelope and the plate were deposited on the layers of Al of equal thicknesses $\Delta_s^{\text{Al}} = \Delta_p^{\text{Al}} = 20 \text{ nm}$. Now the gradient of the additional force can be calculated by applying (13) to each pair of material layers forming the spherical envelope and the plate taking into account the separation distances between each pair of material layers

$$\begin{aligned} \frac{\partial F_{\text{add}}(a)}{\partial a} &= \frac{\pi}{m^2 m_H^2} \int_1^\infty du \frac{\sqrt{u^2 - 1}}{u^2} e^{-2m_a a u} \\ &\times X_p(m_a u) X_s(m_a u), \end{aligned} \quad (16)$$

where

$$\begin{aligned} X_p(z) &\equiv C_{\text{Au}} \left(1 - e^{-2z\Delta_p^{\text{Au}}} \right) \\ &+ C_{\text{Al}} e^{-2z\Delta_p^{\text{Au}}} \left(1 - e^{-2z\Delta_p^{\text{Al}}} \right) + C_{\text{sa}} e^{-2z(\Delta_p^{\text{Au}} + \Delta_p^{\text{Al}})}, \\ X_s(z) &\equiv C_{\text{Au}} \left[\Phi(R, z) - e^{-2z\Delta_s^{\text{Au}}} \Phi(R - \Delta_s^{\text{Au}}, z) \right] \\ &+ C_{\text{Al}} e^{-2z\Delta_s^{\text{Au}}} \left[\Phi(R - \Delta_s^{\text{Au}}, z) \right. \\ &\quad \left. - e^{-2z\Delta_s^{\text{Al}}} \Phi(R - \Delta_s^{\text{Au}} - \Delta_s^{\text{Al}}, z) \right] \\ &+ C_g e^{-2z(\Delta_s^{\text{Au}} + \Delta_s^{\text{Al}})} \left[\Phi(R - \Delta_s^{\text{Au}} - \Delta_s^{\text{Al}}, z) \right. \\ &\quad \left. - e^{-2z\Delta_s^g} \Phi(R - \Delta_s^{\text{Au}} - \Delta_s^{\text{Al}} - \Delta_s^g, z) \right]. \end{aligned} \quad (17)$$

In these equations, the thickness of the sapphire plate was put equal to infinity, as it does not influence the result. The coefficients C_{Au} , C_{Al} , C_g and C_{sa} are defined in Eq. (15) which should be applied to the atoms Au and Al and to the molecules of glass and sapphire [the densities of these materials entering (15) are ρ_{Au} , ρ_{Al} , ρ_g and ρ_{sa} ; they can be found in the tables].

Taking into account that no additional force was observed in the experiment [36, 37] within the measurement error, one can write

$$\frac{\partial F_{\text{add}}(a)}{\partial a} \leq \Delta F'_C(a). \quad (18)$$

Numerical analysis of this equation leads to new constraints on the interaction constants g_{ap} and g_{an} . The strongest constraints are obtained at the shortest experimental separation $a_1 = 235$ nm. At this separation distance the experimental error determined at a 67% confidence level is $\Delta F'_C(a_1) \equiv \Delta_1 F'_C = 0.5 \mu\text{N/m}$ [36]. In Fig. 2 we show these constraints by the solid line under the assumption $g_{ap} = g_{an}$ (see [13] for the alternative assumptions). The region of the plane above the line is excluded, and the region below the line is allowed. The comparison of the solid line in Fig. 2 with the line in Fig. 1 shows that the constraints following from measurements of the gradient of the Casimir force are stronger than those obtained from measurements of the Casimir-Polder force. The largest strengthening by a factor of 170 is achieved for the axion mass $m_a = 0.3$ eV.

Similar results can be obtained [13] from the measurement data of experiment with a Au-coated spherical envelope of $R = 64.1 \mu\text{m}$ radius and a Ni-coated plate [38]. The gradient of the additional force due to two-axion exchange is again given by (16), where $X_s(z)$ is presented in (17) and $X_p(z)$ takes a more simple form due to the absence of an Al layer below a Ni coating

$$X_p(z) = C_{\text{Ni}} \left(1 - e^{-2z\Delta_p^{\text{Ni}}} \right) + C_{\text{Si}} e^{-2z\Delta_p^{\text{Ni}}}. \quad (19)$$

Here, $\Delta_p^{\text{Ni}} = 154$ nm and C_{Ni} can be calculated using (15).

The constraints on the coupling constants of axions to nucleons can be again obtained from (18). The strongest constraints follow at the shortest separation equal to $a_1 = 220$ nm in this experiment. The respective total experimental error determined at a 67% confidence level is $\Delta_1 F'_C = 0.79 \mu\text{N/m}$ [38]. The constraints obtained under the condition $g_{ap} = g_{an}$ are shown by the long-dashed line in Fig. 2. As can be seen in Fig. 2, the constraints following from the experiment with Au-Ni test bodies are up to a factor 1.5 weaker than those obtained from the experiment with Au-Au test bodies. The main reason is the smaller density of Ni, as compared with Au.

In the third experiment, a Ni-coated spherical envelope of $R = 61.71 \mu\text{m}$ radius and a Ni-coated plate were used [39, 40]. The additional force can be again expressed by (16). In this case, however, the functions $X_p(z)$ and $X_s(z)$ are more complicated than in the previously

considered experiments because for technological purposes there were two additional layers (Al and Cr) below the Ni coating on both a spherical envelope and on a plate (see [13] for explicit expressions).

The constraints on $g_{ap} = g_{an}$ were again obtained from (18). The strongest constraints follow at the shortest separation distance ($a_1 = 223$ nm in this case). The total experimental error determined at a 67% confidence level at the shortest separation is $\Delta_1 F'_C = 1.2 \mu\text{N/m}$ [38]. The obtained constraints are shown by the short-dashed line in Fig. 2. They are slightly weaker than those following from the experiments with Au-Au and Au-Ni test bodies. This is again explained by the smaller density of Ni in comparison with that of Au (see Section 7 for comparison with other laboratory constraints).

V. CONSTRAINTS ON AN AXION FROM MEASUREMENTS OF THE CASIMIR PRESSURE BY MEANS OF MICROMACHINED OSCILLATOR

The Casimir pressure $P_C(a)$ between two parallel Au-coated plates was determined from dynamic measurements performed in sphere-plate geometry using a micromechanical torsional oscillator [41, 42]. A sapphire sphere and a Si plate of thickness $D = 5 \mu\text{m}$ were coated with the layers of Cr of equal thickness $\Delta_s^{\text{Cr}} = \Delta_p^{\text{Cr}} = 10$ nm. The outer layers of Au were of thicknesses $\Delta_s^{\text{Au}} = 180$ nm on the sphere and $\Delta_p^{\text{Au}} = 210$ nm on the plate. The resulting radius of the sphere was measured to be $R = 151.3 \mu\text{m}$. The experimental results for the Casimir pressure between two parallel plates spaced a apart were found to be in agreement with the predictions of the Lifshitz theory in the limits of the total experimental error in the pressure measurements $\Delta P_C(a)$ determined at a 95% confidence level. Here, we recalculate this error to a 67% confidence level in order to obtain constraints comparable with those following from other experiments. The theoretical results were obtained with omitted contribution of the relaxation properties of free electrons (taking these properties into account leads to theoretical predictions excluded by the measurement data [23, 24, 41, 42]).

The additional effective pressure between two parallel plates due to two-axion exchange between nucleons of a sphere and a plate can be calculated by the additive summation using

the interaction potential (3) (see [14] for details). The result is the following [14]:

$$P_{\text{add}}(a) = -\frac{1}{2m^2m_{\text{H}}^2R} \int_1^\infty du \frac{\sqrt{u^2-1}}{u^2} \times e^{-2m_a a u} \tilde{X}_p(m_a u) \tilde{X}_s(m_a u), \quad (20)$$

where

$$\begin{aligned} \tilde{X}_p(z) &\equiv C_{\text{Au}} \left(1 - e^{-2z\Delta_p^{\text{Au}}}\right) \\ &+ C_{\text{Cr}} e^{-2z\Delta_p^{\text{Au}}} \left(1 - e^{-2z\Delta_p^{\text{Cr}}}\right) \\ &+ C_{\text{Si}} e^{-2z(\Delta_p^{\text{Au}} + \Delta_p^{\text{Cr}})} \left(1 - e^{-2zD}\right), \quad (21) \\ \tilde{X}_s(z) &\equiv C_{\text{Au}} \left[\Phi(R, z) - e^{-2z\Delta_s^{\text{Au}}} \Phi(R - \Delta_s^{\text{Au}}, z)\right] \\ &+ C_{\text{Cr}} e^{-2z\Delta_s^{\text{Au}}} \left[\Phi(R - \Delta_s^{\text{Au}}, z) \right. \\ &\quad \left. - e^{-2z\Delta_s^{\text{Cr}}} \Phi(R - \Delta_s^{\text{Au}} - \Delta_s^{\text{Cr}}, z)\right] \\ &+ C_{sa} e^{-2z(\Delta_s^{\text{Au}} + \Delta_s^{\text{Cr}})} \Phi(R - \Delta_s^{\text{Au}} - \Delta_s^{\text{Cr}}, z). \end{aligned}$$

The function $\Phi(r, z)$ used here is given in (14). The coefficients C_{Au} , C_{Cr} , C_{Si} , and C_{sa} are the same as used above. All of them are expressed by (15), as applied to respective materials.

The constraints on the axion-nucleon interaction constants were found from the inequality

$$|P_{\text{add}}(a)| \leq \Delta P_C(a). \quad (22)$$

For different regions of axion masses the strongest constraints follow from (22) at different separation distances. Thus, within the regions $m_a < 0.1 \text{ eV}$, $0.1 \text{ eV} \leq m_a < 0.5 \text{ eV}$ and $0.5 \text{ eV} \leq m_a < 15 \text{ eV}$ the strongest constraints were obtained at $a = 300$, 200 and 162 nm , respectively. At these separations the total experimental errors in measurements of the Casimir pressure recalculated to a 67% confidence level were equal to 0.22 , 0.38 , and 0.55 mPa , respectively. In Fig. 3 the obtained constraints are shown by the solid line under the condition $g_{ap} = g_{an}$. They are stronger than the constraints following from measurements of the Casimir-Polder force (see Fig. 1) and from measurements of the gradient of the Casimir force between Au-Au surfaces (see the solid line in Fig. 2). Thus, at $m_a = 1 \text{ eV}$ the constraints of Fig. 3 are stronger by a factor of 3.2 than the strongest constraints of Fig. 2 shown by the solid line (a more detailed comparison is contained in Section 7).

VI. CONSTRAINTS ON AN AXION FROM MEASUREMENTS OF THE CASIMIR FORCE BETWEEN CORRUGATED SURFACES

Several measurements of the Casimir interaction between a sphere and a plate were performed in the case when the surface of at least one test body is not smooth, but covered with the longitudinal corrugations [43–50]. The shape of the corrugations was either sinusoidal [43, 44, 47–50] or rectangular [45, 46] (in the latter case the sphere was smooth, and only the plate was corrugated). If both the test bodies are corrugated and some nonzero phase shift between corrugations is present, there is not only the normal Casimir force acting perpendicular to the surfaces, but the lateral Casimir force as well [43, 44, 47, 48]. Here we consider the constraints on axion-nucleon coupling constants obtained [15] from measurements of the normal [49, 50] and lateral [47, 48] Casimir force between sinusoidally corrugated Au-coated surfaces (experiments [43, 44] are less precise, and experiments [45, 46] use the rectangular corrugated Si plates and lead to weaker constraints due to a smaller density of Si).

We begin with an experiment on measuring the lateral Casimir force between sinusoidally corrugated surfaces of a sphere and a plate [47, 48]. The corrugation axes of the longitudinal corrugations on both bodies were kept parallel, and there was some phase shift φ_0 between corrugations. The period of corrugations was $\Lambda = 574.4$ nm. Measurements of the lateral Casimir force as a function of the phase shift were performed over the region of separations between the mean levels of corrugations from 120 to 190 nm. The corrugation amplitudes were $A_1 = 85.4$ nm and $A_2 = 13.7$ nm on the plate and on the sphere, respectively. The plate was made of a hard epoxy and coated with a layer of Au of thickness $\Delta_p^{\text{Au}} = 300$ nm. The sphere was made of polystyrene and coated with a layer of Cr of $\Delta_s^{\text{Cr}} = 10$ nm thickness and then with a layer of Au of $\Delta_s^{\text{Au}} = 50$ nm thickness. The outer radius of the sphere was measured to be $R = 97.0$ μm . The measurement results were compared with theoretical predictions of the scattering theory (which generalizes the Lifshitz theory for the case of arbitrary shaped bodies) and demonstrated good agreement in the limits of the experimental error $\Delta F_C^{\text{lat}}(a)$ [47, 48].

The additional lateral force due to two-axion exchange between sinusoidally corrugated surfaces of a sphere and a plate can be calculated using (3). The maximum amplitude of

this force, which is obtained at the phase shift $\varphi_0 = \pi/2$, takes the form [15]

$$\begin{aligned}
\max |F_{\text{add}}^{\text{lat}}(a)| &= \frac{\pi^2 R C_{\text{Au}}}{m_a m^2 m_{\text{H}}^2} \frac{A_1 A_2}{\Lambda \sqrt{A_1^2 + A_2^2}} \\
&\times \int_1^\infty du \frac{\sqrt{u^2 - 1}}{u^3} e^{-2m_a u a} I_1 \left(2m_a u \sqrt{A_1^2 + A_2^2} \right) \\
&\times (1 - e^{-2m_a u \Delta_p^{\text{Au}}}) \left[C_{\text{Au}} + (C_{\text{Cr}} - C_{\text{Au}}) \right. \\
&\left. \times e^{-2m_a u \Delta_s^{\text{Au}}} - C_{\text{Cr}} e^{-2m_a u (\Delta_s^{\text{Au}} + \Delta_s^{\text{Cr}})} \right]. \tag{23}
\end{aligned}$$

Here, the hard epoxy and polystyrene would lead to negligibly small contributions to the force due to two-axion exchange. Because of this, only metallic coatings were taken into account in (23).

The constraints on an axion can be obtained from the inequality

$$\max |F_{\text{add}}^{\text{lat}}(a)| \leq \Delta F_C^{\text{lat}}(a), \tag{24}$$

where the left-hand side is given by (23). For axion-like particles with masses $m_a < 20$ eV, the strongest constraints are obtained from the measure of agreement between experiment and theory at $a = 124.7$ nm. At this separation the total experimental error recalculated to a 67% confidence level for convenience in comparison with other experiments is $\Delta F_C^{\text{lat}} = 2.4$ pN (note that according to a conservative estimation, the total experimental error calculated in [47, 48] at a 95% confidence level is by a factor of 2 larger than the same error found at a 67% confidence level). The constraints on $g_{ap} = g_{an}$ obtained from (24) at $a = 124.7$ nm are shown by the solid line in Fig. 4, where the region of the plane above the line is excluded and the region below the line is allowed. Note that this line is slightly different from the respective lines in Fig. 2(a,b) in [15] because it was plotted there at the 95% confidence level.

We now turn our attention to the experiment on measuring the normal Casimir force between a sinusoidally corrugated Au-coated polystyrene sphere of $R = 99.6$ μm radius and a sinusoidally corrugated Au-coated plate made of hard epoxy [49, 50]. This experiment was performed at different angles between the longitudinal corrugations on the sphere and on the plate varying from 0 to 2.4°. There was no phase shift between corrugations on both bodies. Below we obtain constraints on the axion-nucleon coupling constants from the measurement data for the case of parallel corrugation axes on the sphere and the plate.

The thicknesses of Au coatings on the sphere and on the plate were $\Delta_s^{\text{Au}} = 110$ nm and $\Delta_p^{\text{Au}} = 300$ nm, respectively. For technological purposes, before depositing the Au coatings, the sphere was first coated with a layer of Cr of thickness $\Delta_s^{\text{Cr}} = 10$ nm and then with a layer of Al of thickness $\Delta_s^{\text{Al}} = 20$ nm. The period of uniaxial sinusoidal corrugations on both bodies was $\Lambda = 570.5$ nm, and the corrugations amplitudes were $A_1 = 40.2$ nm and $A_2 = 14.6$ nm on the plate and on the sphere, respectively. The measurement results were compared with theoretical predictions of the scattering theory and found in good agreement within the limits of the total experimental error.

The additional normal force acting between a sphere and a plate due to two-axion exchange was again calculated [15] using (3)

$$\begin{aligned}
F_{\text{add}}^{\text{nor}}(a) = & -\frac{\pi R C_{\text{Au}}}{2m_a m^2 m_{\text{H}}^2} \int_1^\infty du \frac{\sqrt{u^2 - 1}}{u^3} e^{-2m_a u a} \\
& \times I_0(2m_a u (A_1 - A_2)) (1 - e^{-2m_a u \Delta_p^{\text{Au}}}) \\
& \times \left[C_{\text{Au}} + (C_{\text{Al}} - C_{\text{Au}}) e^{-2m_a u \Delta_s^{\text{Au}}} \right. \\
& + (C_{\text{Cr}} - C_{\text{Al}}) e^{-2m_a u (\Delta_s^{\text{Au}} + \Delta_s^{\text{Al}})} \\
& \left. - C_{\text{Cr}} e^{-2m_a u (\Delta_s^{\text{Au}} + \Delta_s^{\text{Al}} + \Delta_s^{\text{Cr}})} \right]. \tag{25}
\end{aligned}$$

The constraints on the axion-nucleon coupling constants $g_{an} = g_{ap}$ were found from the inequality

$$|F_{\text{add}}^{\text{nor}}(a)| \leq \Delta F_C^{\text{nor}}(a). \tag{26}$$

The strongest constraints follow from (26) at the shortest separation distance $a_1 = 127$ nm where the total experimental error determined at a 67% confidence level is equal to $\Delta F_C^{\text{nor}}(a_1) = 0.94$ pN [49, 50].

In Fig. 4 the obtained constraints under a condition $g_{an} = g_{ap}$ are shown by the dashed line. It can be seen that for $m_a < 5.3$ eV they are stronger than those following from measurements of the lateral Casimir force (the solid line), but become weaker than the latter for larger axion masses.

VII. COMPARISON BETWEEN DIFFERENT LABORATORY CONSTRAINTS

It is interesting to compare all discussed above constraints, obtained from measurements of the Casimir interaction, between themselves and with other laboratory constraints on

axion to nucleon coupling constants. Such a comparison is performed in Fig. 5 over the wide range of axion masses from 10^{-10} to 20 eV. The constraints on g_{an} obtained [51] by means of a magnetometer using spin-polarized K and ^3He atoms are shown by the solid line 1. These constraints are applicable in the region of m_a from 10^{-10} to 6×10^{-6} eV. The solid line 2 indicates the constraints obtained [52] from the recent Cavendish-type experiment [53] in the region from $m_a = 10^{-6}$ to 6×10^{-2} eV. The weaker constraints found [25] from the older Cavendish-type experiments [54, 55] and from the Eötvos-type experiment [56], respectively, are shown by the dashed lines 3 and 4 (these and the following constraints are obtained under a condition $g_{an} = g_{ap}$). These constraints cover the region of m_a from 10^{-8} eV to 4×10^{-5} eV (line 3) and to 10^{-5} eV (line 4). The lines 5–8 are obtained [12–15] from measurements of the Casimir interaction. They are discussed in this paper. The line 5 reproduces the line in Fig. 3 obtained for m_a from 10^{-3} to 15 eV from measurements of the Casimir pressure (see Section 5). The dashed lines 6 and 7 reproduce the solid line in Fig. 2 and the line in Fig. 1 found in the region from 3×10^{-5} to 1 eV from measurements of the gradient of the Casimir force between Au-Au surfaces and in the region from 10^{-4} to 0.3 eV from measurements of the Casimir-Polder force, respectively (see Sections 4 and 3). Finally, the line 8 reproduces the solid line in Fig. 4 found in the region of m_a from 1 to 20 eV. It follows from measurements of the lateral Casimir force between corrugated surfaces discussed in Section 6 (measurements of the normal Casimir force between sinusoidally corrugated surfaces lead to weaker constraints than those shown in Fig. 5).

The strength of almost all laboratory constraints shown in Fig 5 (with exception of that shown by line 1) monotonically decreases with increase of the axion mass m_a . If one introduces the Compton wavelength of an axion $\lambda_a = 1/m_a$, it is correct to say that the strength of almost all constraints (and all of those following from measurements of the gravitational and Casimir interactions) decreases with decreasing λ_a . The same is true for the Yukawa-type corrections to Newton’s law of gravitation (4) whose strength decreases with decreasing interaction range λ (see the next section). This property likens the interaction potentials (3) and (4) and specifies the interaction range where the most strong constraints on respective hypothetical forces can be obtained from experiments on measuring the Casimir interaction.

The vertical lines in Fig. 5 indicate the region from $m_a = 10^{-5}$ to 10^{-2} eV, which is often called an axion window [57]. As can be seen in Fig. 5, experiments measuring the Casimir

interaction lead to strengthening of the laboratory constraints on axion to nucleon coupling constants near the upper border of the axion window and also for larger axion masses.

VIII. CONSTRAINTS ON CORRECTIONS TO NEWTON'S LAW OF GRAVITATION

The constraints on corrections to the Newton law of gravitation described by the potentials (4) and (5) can be obtained from the gravitational experiments of Eötvös- and Cavendish-type and from measurements of the Casimir interaction. As explained in Section 1, measurements of the Casimir force have long been used for constraining hypothetical interactions of both Yukawa and power type. Because of this, here we only briefly present the obtained results and indicate regions where measurements of the Casimir force lead to the most strong constraints, as compared to gravitational experiments.

The Yukawa-type interaction potential between the test bodies used in experiments on measuring the Casimir force is obtained by the integration of (4) over the volumes of bodies. In so doing, at submicrometer separations the Newton gravitational force turns out to be negligibly small, as compared to the error of force measurements. Similar to the case of axion considered above, the constraints on the constants of Yukawa-type interaction α and λ are obtained from a condition that this interaction was not experimentally observed in the limits of the experimental error in measurements of the Casimir interaction.

In Fig. 6 we present the strongest constraints on the Yukawa interaction constant α in the micrometer and submicrometer interaction range λ obtained from measurements of the Casimir interaction. The line 1 in Fig. 6 was obtained [18] from measurements of the lateral Casimir force between sinusoidally corrugated surfaces of a sphere and a plate [47, 48] (see Section 6). It presents the strongest constraints on the Yukawa-type corrections to Newton's law of gravitation within the interaction range from $\lambda = 1.6$ to 11.6 nm. The line 2 shows constraints found [21] from measuring the normal Casimir force between sinusoidally corrugated surfaces at the angle between corrugations equal to 2.4° [49, 50] (see Section 6). These constraints are the strongest ones in the interaction range from 11.6 to 17.2 nm. The constraints obtained from measurements of the Casimir pressure by means of a micromachined torsional oscillator (see Section 5) are indicated by the line 3. They are the strongest ones for $17.2 \text{ nm} < \lambda < 89 \text{ nm}$. At larger λ the most strong

constraints shown by the line 4 follow from the so-called Casimir-less experiment [58], where the Casimir force was nullified by using the difference force measurement scheme. These constraints are the strongest ones up to $\lambda = 891$ nm. The constraints of the line 5 are found [59] from measurements of the Casimir force between Au-coated surfaces of a plate and a spherical lens of large radius. They are the strongest ones up to $\lambda = 3.16$ μ m. For larger λ the strongest constraints on the Yukawa-type corrections to Newton's gravitational law follow from the Cavendish-type experiments. The first constraints of such kind are indicated by the line 6 [60, 61]. Thus, measurements of the Casimir interaction lead to the most strong constraints on non-Newtonian gravity over a wide interaction range from 1.6 nm to a few micrometers. As can be seen in Fig. 6, the strength of all constraints decreases with decreasing λ , i.e., with increasing mass of a hypothetical particle which initiates the additional interaction of Yukawa-type. This is similar to the case of an axion considered in Sections 3–6.

Constraints on the power-type corrections to Newton's law of gravitation (5) follow from the gravitational experiments of Eötvös and Cavendish type [8] and from measurements of the Casimir force [17, 30]. At the present time the most strong constraints follow from the Eötvös-type experiments ($|\Lambda_1| \leq 1 \times 10^{-9}$ [62] and $|\Lambda_2| \leq 4 \times 10^8$ [56]) and from the Cavendish-type experiments ($|\Lambda_3| \leq 1.3 \times 10^{20}$ [52], $|\Lambda_4| \leq 4.9 \times 10^{31}$ [52], and $|\Lambda_5| \leq 1.5 \times 10^{43}$ [52]). Note that [52] uses another parametrization for the power-type corrections to Newtonian gravitation.

IX. CONCLUSIONS AND DISCUSSION

In the foregoing, we have considered the constraints on axion to nucleon couplings following from laboratory experiments on measuring the Casimir interaction. The obtained constraints are quite competitive in the region of axion masses from 10^{-3} to 20 eV. The most strong of them follow from a dynamic determination of the Casimir pressure between two parallel plates and from measurement of the lateral Casimir force between sinusoidally corrugated surfaces. All these constraints were derived by considering the process of two-axion exchange between two nucleons. This process is of the lowest order contributing to the force acting between unpolarized test bodies. The obtained constraints were compared with those following from other laboratory experiments.

We have also compared the constraints on an axion with previously obtained constraints on corrections to the Newton law of gravitation of Yukawa and power type. The most strong constraints of this kind following from measurements of the Casimir interaction are collected. In the interaction range below a few micrometers they are stronger than the constraints on Yukawa-type corrections to Newton's law following from the gravitational experiments of Eötvös and Cavendish type.

In future it would be interesting to perform measurements of the Casimir interaction between two polarized test bodies. This would lead to an additional force due to exchange of one axion between protons and neutrons and, as a consequence, to much stronger constraints on the axion to nucleon coupling constants.

-
- [1] S. Weinberg, Phys. Rev. Lett. **40**, 223 (1978).
 - [2] F. Wilczek, Phys. Rev. Lett. **40**, 279 (1978).
 - [3] R. D. Peccei and H. R. Quinn, Phys. Rev. Lett. **38**, 1440 (1977).
 - [4] J. E. Kim, Phys. Rep. **150**, 1 (1987).
 - [5] Yu. N. Gnedin, Int. J. Mod. Phys. A **17**, 4251 (2002).
 - [6] K. Baker *et al.* Ann. Phys. (Berlin) **525**, A93 (2013).
 - [7] S. Dimopoulos and G. F. Giudice, Phys. Lett. B **379**, 105 (1996).
 - [8] E. Fischbach and C. L. Talmadge, *The Search for Non-Newtonian Gravity* (Springer, New York, 1999).
 - [9] I. Antoniadis, N. Arkani-Hamed, S. Dimopoulos, and G. Dvali, Phys. Lett. B **436**, 257 (1998).
 - [10] N. Arkani-Hamed, S. Dimopoulos, and G. Dvali, Phys. Rev. D **59**, 086004 (1999).
 - [11] E. G. Adelberger, J. H. Gundlach, B. R. Heckel, S. Hoedl, and S. Schlamminger, Part. Nucl. Phys. **62**, 102 (2009).
 - [12] V. B. Bezerra, G. L. Klimchitskaya, V. M. Mostepanenko, and C. Romero, Phys. Rev. D **89**, 035010 (2014).
 - [13] V. B. Bezerra, G. L. Klimchitskaya, V. M. Mostepanenko, and C. Romero, Phys. Rev. D **89**, 075002 (2014).
 - [14] V. B. Bezerra, G. L. Klimchitskaya, V. M. Mostepanenko, and C. Romero, Eur. Phys. J. C **74**, 2859 (2014).

- [15] V. B. Bezerra, G. L. Klimchitskaya, V. M. Mostepanenko, and C. Romero, Phys. Rev. D **90**, 055013 (2014).
- [16] V. A. Kuzmin, I. I. Tkachev, and M. E. Shaposhnikov, Pis'ma v ZhETF **36**, 49 (1982) [JETP Lett. **36**, 59 (1982)].
- [17] V. M. Mostepanenko and I. Yu. Sokolov, Phys. Lett. A **125**, 405 (1987).
- [18] V. B. Bezerra, G. L. Klimchitskaya, V. M. Mostepanenko, and C. Romero, Phys. Rev. D **81**, 055003 (2010).
- [19] V. B. Bezerra, G. L. Klimchitskaya, V. M. Mostepanenko, and C. Romero, Phys. Rev. D **83**, 075004 (2011).
- [20] G. L. Klimchitskaya, U. Mohideen, and V. M. Mostepanenko, Phys. Rev. D **86**, 065025 (2012).
- [21] G. L. Klimchitskaya, U. Mohideen, and V. M. Mostepanenko, Phys. Rev. D **87**, 125031 (2013).
- [22] G. L. Klimchitskaya and V. M. Mostepanenko, Grav. Cosmol. **20**, 3 (2014).
- [23] M. Bordag, G. L. Klimchitskaya, U. Mohideen, and V. M. Mostepanenko, *Advances in the Casimir Effect* (Oxford University Press, Oxford, 2009).
- [24] G. L. Klimchitskaya, U. Mohideen, and V. M. Mostepanenko, Rev. Mod. Phys. **81**, 1827 (2009).
- [25] E. G. Adelberger, E. Fischbach, D. E. Krause, and R. D. Newman, Phys. Rev. D **68**, 062002 (2003).
- [26] A. Bohr and B. R. Mottelson, *Nuclear Structure* (Benjamin, New York, 1969), Vol. 1.
- [27] S. D. Drell and K. Huang, Phys. Rev. **91**, 1527 (1953).
- [28] F. Ferrer and M. Nowakowski, Phys. Rev. D **59**, 075009 (1999).
- [29] E. Fischbach, Ann. Phys. (N.Y.) **247**, 213 (1996).
- [30] V. M. Mostepanenko and I. Yu. Sokolov, Phys. Rev. D **47**, 2882 (1993).
- [31] V. M. Mostepanenko and I. Yu. Sokolov, Sov. J. Nucl. Phys. **46**, 685 (1987).
- [32] L. Randall and R. Sundrum, Phys. Rev. Lett. **83**, 3370 (1999).
- [33] L. Randall and R. Sundrum, Phys. Rev. Lett. **83**, 4690 (1999).
- [34] J. M. Obrecht, R. J. Wild, M. Antezza, L. P. Pitaevskii, S. Stringari, and E. A. Cornell, Phys. Rev. Lett. **98**, 063201 (2007).
- [35] G. L. Klimchitskaya and V. M. Mostepanenko, J. Phys. A: Math. Theor. **41**, 312002 (2008).
- [36] C.-C. Chang, A. A. Banishev, R. Castillo-Garza, G. L. Klimchitskaya, V. M. Mostepanenko, and U. Mohideen, Phys. Rev. B **85**, 165443 (2012).

- [37] A. A. Banishev, C.-C. Chang, R. Castillo-Garza, G. L. Klimchitskaya, V. M. Mostepanenko, and U. Mohideen, *Int. J. Mod. Phys. A* **27**, 1260001 (2012).
- [38] A. A. Banishev, C.-C. Chang, G. L. Klimchitskaya, V. M. Mostepanenko, and U. Mohideen, *Phys. Rev. B* **85**, 195422 (2012).
- [39] A. A. Banishev, G. L. Klimchitskaya, V. M. Mostepanenko, and U. Mohideen, *Phys. Rev. Lett.* **110**, 137401 (2013).
- [40] A. A. Banishev, G. L. Klimchitskaya, V. M. Mostepanenko, and U. Mohideen, *Phys. Rev. B* **88**, 155410 (2013).
- [41] R. S. Decca, D. López, E. Fischbach, G. L. Klimchitskaya, D. E. Krause, and V. M. Mostepanenko, *Phys. Rev. D* **75**, 077101 (2007).
- [42] R. S. Decca, D. López, E. Fischbach, G. L. Klimchitskaya, D. E. Krause, and V. M. Mostepanenko, *Eur. Phys. J. C* **51**, 963 (2007).
- [43] F. Chen, U. Mohideen, G. L. Klimchitskaya, and V. M. Mostepanenko, *Phys. Rev. Lett.* **88**, 101801 (2002).
- [44] F. Chen, U. Mohideen, G. L. Klimchitskaya, and V. M. Mostepanenko, *Phys. Rev. A* **66**, 032113 (2002).
- [45] H. B. Chan, Y. Bao, J. Zou, R. A. Cirelli, F. Klemens, W. M. Mansfield, and C. S. Pai, *Phys. Rev. Lett.* **101**, 030401 (2008).
- [46] Y. Bao, R. Guérout, J. Lussange, A. Lambrecht, R. A. Cirelli, F. Klemens, W. M. Mansfield, C. S. Pai, and H. B. Chan, *Phys. Rev. Lett.* **105**, 250402 (2010).
- [47] H.-C. Chiu, G. L. Klimchitskaya, V. N. Marachevsky, V. M. Mostepanenko, and U. Mohideen, *Phys. Rev. B* **80**, 121402(R) (2009).
- [48] H.-C. Chiu, G. L. Klimchitskaya, V. N. Marachevsky, V. M. Mostepanenko, and U. Mohideen, *Phys. Rev. B* **81**, 115417 (2010).
- [49] A. A. Banishev, J. Wagner, T. Emig, R. Zandi, and U. Mohideen, *Phys. Rev. Lett.* **110**, 250403 (2013).
- [50] A. A. Banishev, J. Wagner, T. Emig, R. Zandi, and U. Mohideen, *Phys. Rev. B* **89**, 235436 (2014).
- [51] G. Vasilakis, J. M. Brown, T. R. Kornack, and M. V. Romalis, *Phys. Rev. Lett.* **103**, 261801 (2009).
- [52] E. G. Adelberger, B. R. Heckel, S. Hoedl, C. D. Hoyle, D. J. Kapner, and A. Upadhye, *Phys.*

- Rev. Lett. **98**, 131104 (2007).
- [53] D. J. Kapner, T. S. Cook, E. G. Adelberger, J. H. Gundlach, B. R. Heckel, C. D. Hoyle, and H. E. Swanson, Phys. Rev. Lett. **98**, 021101 (2007).
- [54] R. Spero, J. K. Hoskins, R. Newman, J. Pellam, and J. Schultz, Phys. Rev. Lett. **44**, 1645 (1980).
- [55] J. K. Hoskins, R. D. Newman, R. Spero, and J. Schultz, Phys. Rev. D **32**, 3084 (1985).
- [56] G. L. Smith, C. D. Hoyle, J. H. Gundlach, E. G. Adelberger, B. R. Heckel, and H. E. Swanson, Phys. Rev. D **61**, 022001 (1999).
- [57] G. G. Raffelt, J. Phys. A: Math. Theor. **40**, 6607 (2007).
- [58] R. S. Decca, D. López, E. Fischbach, D. E. Krause, and C. R. Jamell, Phys. Rev. Lett. **94**, 240401 (2005).
- [59] M. Masuda and M. Sasaki, Phys. Rev. Lett. **102**, 171101 (2009).
- [60] S. J. Smullin, A. A. Geraci, D. M. Weld, J. Chiaverini, S. Holmes, and A. Kapitulnik, Phys. Rev. D **72**, 122001 (2005).
- [61] A. A. Geraci, S. J. Smullin, D. M. Weld, J. Chiaverini, and A. Kapitulnik, Phys. Rev. D **78**, 022002 (2008).
- [62] J. H. Gundlach, G. L. Smith, E. G. Adelberger, B. R. Heckel, and H. E. Swanson, Phys. Rev. Lett. **78**, 2523 (1997).

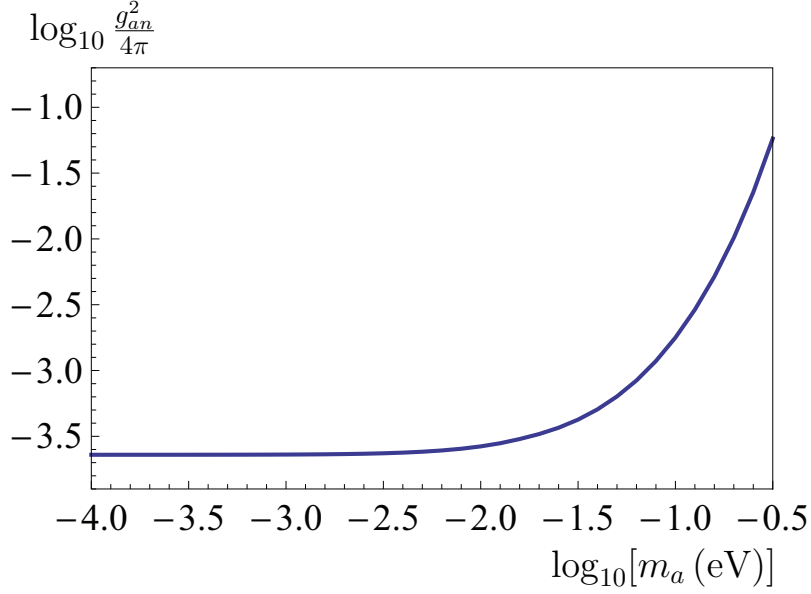


FIG. 1: Constraints on the coupling constants of an axion with a proton and a neutron following from measurements of the thermal Casimir-Polder force are shown as a function of the axion mass. The region of the plane above the line is prohibited and below the line is allowed.

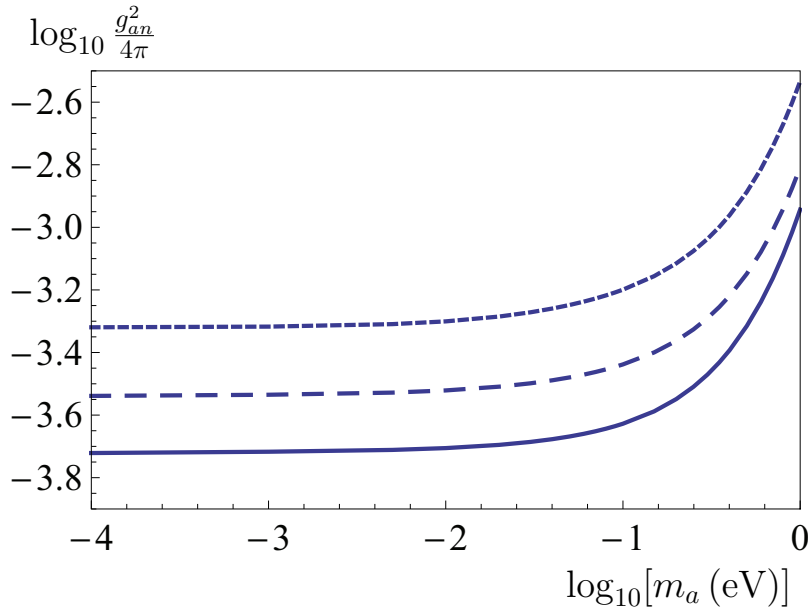


FIG. 2: Constraints on the coupling constants of an axion with a proton and a neutron following from measurements of the gradient of the Casimir force between Au-Au, Au-Ni and Ni-Ni surfaces are shown as functions of the axion mass by the solid, long-dashed and short-dashed lines, respectively. The regions of the plane above the lines are prohibited and below the lines are allowed.

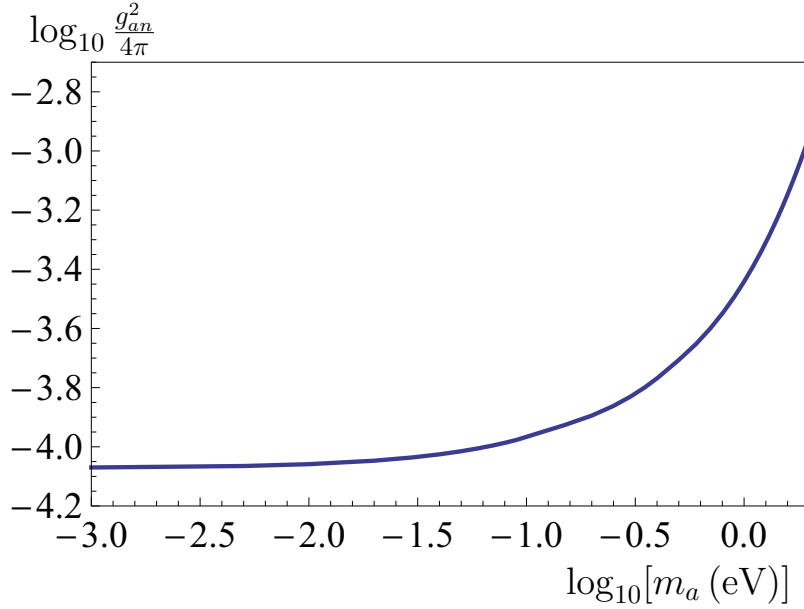


FIG. 3: Constraints on the coupling constants of an axion with a proton and a neutron following from dynamic determination of the Casimir pressure between two parallel Au plates are shown as a function of the axion mass. The region of the plane above the line is prohibited and below the line is allowed.

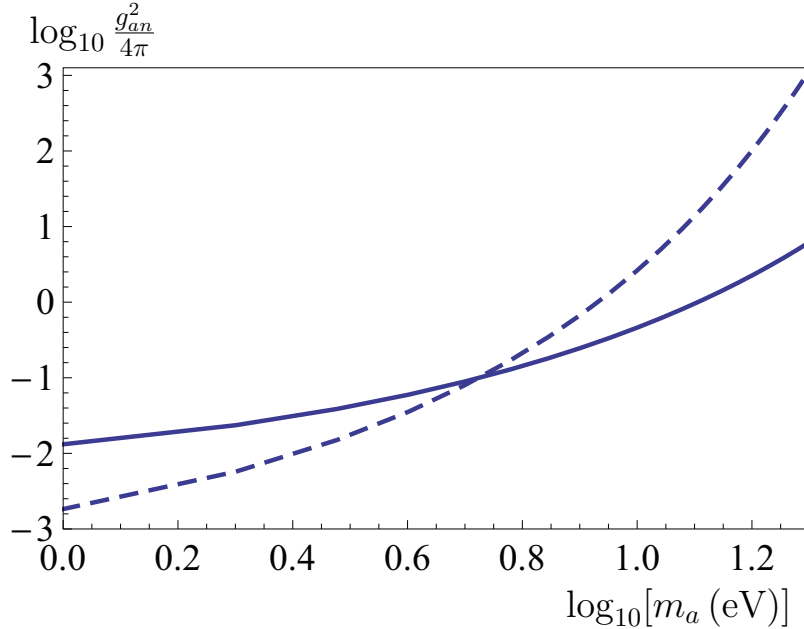


FIG. 4: Constraints on the coupling constants of an axion with a proton and a neutron following from measurements of the lateral (the solid line) and normal (the dashed line) Casimir forces between sinusoidally corrugated surfaces are shown as functions of the axion mass. The regions of the plane above the lines are prohibited and below the lines are allowed.

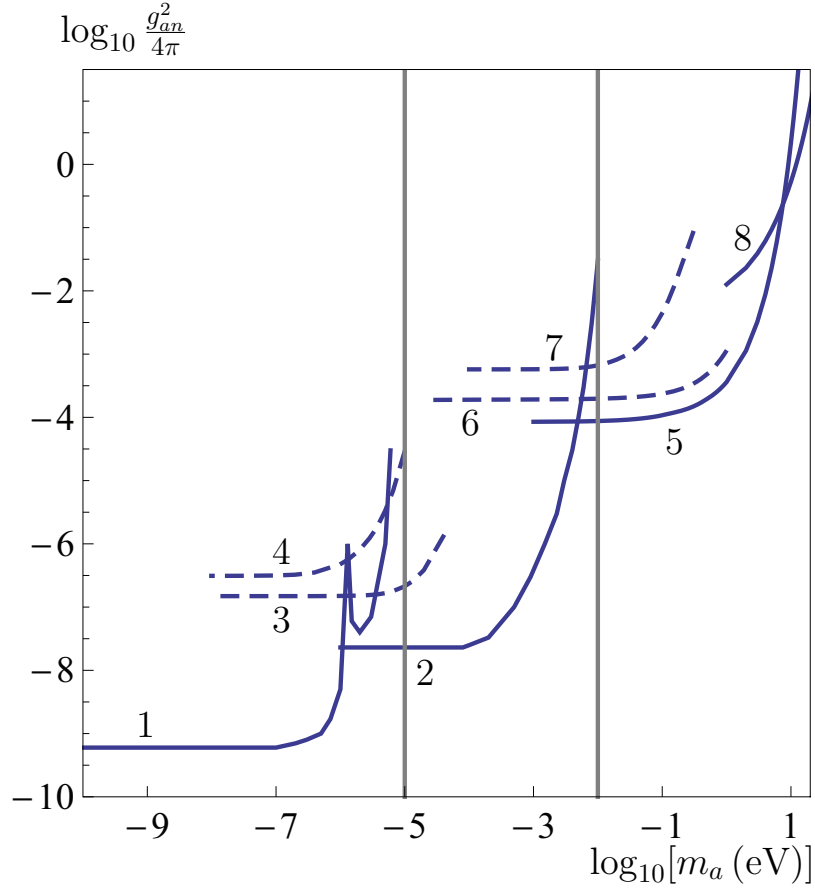


FIG. 5: Different laboratory constraints on the coupling constant of an axion with a neutron following from the magnetometer measurements (the line 1), from the Cavendish- and Eötvös-type experiments (the lines 2–4), from measurements of the Casimir pressure (the line 5), of the gradient of the Casimir force (the line 6), of the Casimir-Polder force (the line 7), and of the lateral Casimir force (the line 8) are shown as functions of the axion mass. The two vertical lines indicate the borders of the axion window. The regions above each line are prohibited and below each line are allowed.

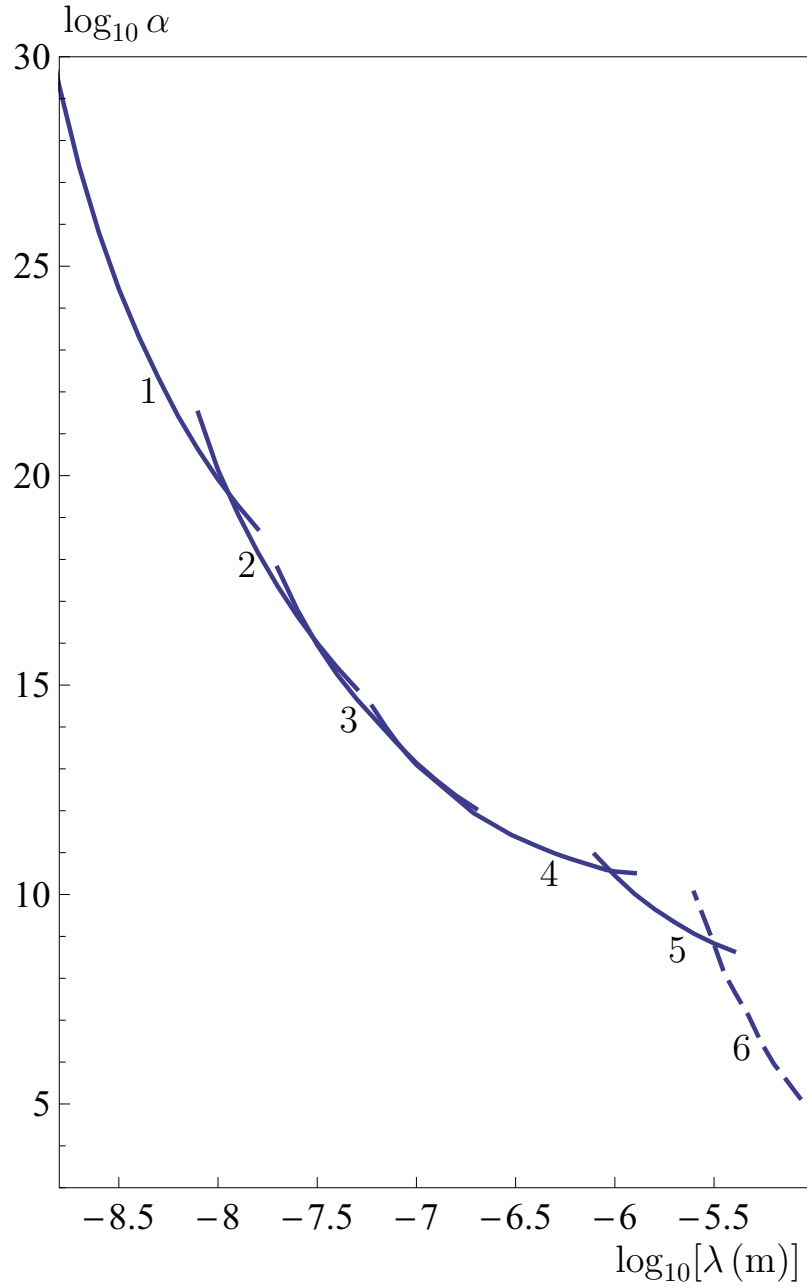


FIG. 6: Constraints on the Yukawa-type corrections to the Newton law of gravitation obtained from measurements of the lateral Casimir force between corrugated surfaces (the line 1), of the normal Casimir force between corrugated surfaces (the line 2), of the Casimir pressure (the line 3), from the Casimir-less experiment (the line 4), from measurements of the Casimir force between a plate and a spherical lens (the line 5), and from the Cavendish-type experiment (the line 6) are shown as functions of the interaction range. The regions of the plane above the lines are prohibited and below the lines are allowed.